



Cite this: *Chem. Sci.*, 2024, 15, 19513 All publication charges for this article have been paid for by the Royal Society of Chemistry

# Steering N/S coordination number to accelerate catecholase-like catalysis over low-coordinated Cu site†

Meng Yuan,<sup>a</sup> Nannan Xia,<sup>b</sup> Ziheng Huang,<sup>a</sup> Chaofeng Huang,<sup>c</sup> Xun Hu  <sup>\*a</sup> and Fei He  <sup>\*a</sup>

Modulation of coordination configuration is crucial for boosting the biomimetic catalytic activity of nanozymes, but remains challenging. Here, we found that the non-first-shell amino group in the ligand was capable of steering the N/S coordination number through remote induction to enable the formation of a low-coordinated  $\text{CuN}_2\text{S}_1$  configuration. This endowed the resulting nanozyme (ATT-Cu) with an upshifted d-band center compared with a control nanozyme (TT-Cu) with  $\text{CuN}_1\text{S}_3$  configuration, enhancing the adsorption capabilities of ATT-Cu for  $\text{O}_2$  and  $\text{H}_2\text{O}_2$  intermediates as well as its affinity for catechol. Additionally, the low-coordinated  $\text{CuN}_2\text{S}_1$  configuration caused more charges to accumulate at the atomic Cu site, which improved the capabilities of ATT-Cu for both donating electrons to oxygen-related species and accepting electrons from catechol. As a result, this ATT-Cu nanozyme with a low-coordinated  $\text{CuN}_2\text{S}_1$  moiety presented a faster initial oxygen reduction step, which in turn accelerated catechol oxidation, thus greatly boosting the catecholase-like activity of ATT-Cu that exceeded those of many catecholase-mimicking artificial enzymes/nanozymes with  $\text{Cu-N}_x\text{O}_y$  sites as well as those of Ce-based, Zr-based and Pt-based nanozymes.

Received 27th July 2024  
Accepted 18th October 2024

DOI: 10.1039/d4sc05014b

rsc.li/chemical-science

## Introduction

Nanozymes with enzyme-like catalytic functions are potential candidates for replacing natural enzymes due to their tunable activities, excellent recyclability and low cost.<sup>1–9</sup> Despite these advantages, the broad application prospects of nanozymes are usually hindered by their poor catalytic activities. To address this challenge, various strategies have been employed to improve the biomimetic catalytic activities of nanozymes. Taking nanozyme-mimicking catechol oxidase (CO) as an example, regulating multinuclearity,<sup>2</sup> chiral microenvironment,<sup>10</sup> coordination saturation<sup>11</sup> and the types of coordination center atoms<sup>12–14</sup> have generally been used to manipulate the catalytic activities of CO-like nanozymes. Despite great advances, many CO-mimicking nanozymes or artificial enzymes, especially those carrying  $\text{M-N}_x\text{O}_y$  moieties (where M represents a metal) as catalytic sites, still exhibit unsatisfactory

activities.<sup>10,15</sup> One possible reason is the strong electronegativity of coordinated N and/or O atoms with small atomic radius, which results in the metal sites either have unsuitable free energy for adsorption/desorption of reaction-related species (including reactants, intermediates and/or products)<sup>16</sup> or inappropriate electron transfer capability for donating and/or accepting electrons.

To overcome these obstacles, a potential solution is to choose a coordinating atom with comparatively large atomic size and weak electronegativity<sup>17</sup> to regulate the interface configuration of the central metal atoms,<sup>16</sup> thus boosting the catalytic activity of CO-mimicking nanozymes by adjusting the electronic state of the metal site to optimize the potential barriers to adsorption/desorption as well as electron transfer capability during biomimetic catalysis. In this regard, using S to partially replace N or O as the coordinating atom may be a promising choice due to its large atomic size and weak electronegativity compared to N and O atoms. However, few CO-mimicking nanozymes with  $\text{M-N}_x\text{S}_y$  or  $\text{M-O}_x\text{S}_y$  moieties have been reported.

With this goal in mind, we herein used the non-first-shell amino group to perturb the N/S coordination number around an atomic Cu center to construct two nanozymes with  $\text{CuN}_2\text{S}_1$  and  $\text{CuN}_1\text{S}_3$  moieties for CO-mimicking catalysis. We found that the low-coordinated  $\text{CuN}_2\text{S}_1$  configuration endowed the resulting nanozyme with an upshifted d-band center, which enhanced the adsorption strength of the Cu site for  $\text{O}_2$  and

<sup>a</sup>School of Material Science and Engineering, University of Jinan, Jinan 250024, China. E-mail: xun.hu@outlook.com; mse\_hef@ujn.edu.cn

<sup>b</sup>State Key Laboratory of Biobased Material and Green Papermaking, Key Laboratory of Pulp & Paper Science and Technology of Shandong Province/Ministry of Education, Qilu University of Technology (Shandong Academy of Sciences), Jinan 250353, China

<sup>c</sup>School of Chemistry and Chemical Engineering/State Key Laboratory Incubation Base for Green Processing of Chemical Engineering, Shihezi University, Shihezi 832000, China

† Electronic supplementary information (ESI) available. See DOI: <https://doi.org/10.1039/d4sc05014b>

H<sub>2</sub>O<sub>2</sub> intermediates as well as the affinity for catechol. Moreover, this low-coordinated CuN<sub>2</sub>S<sub>1</sub> moiety promoted charge accumulation over the atomic Cu center, enabling the resulting nanozyme to more easily donate electrons to oxygen-related species and accept electrons from catechol. Accordingly, when applied to CO-mimicking catalysis, the unsaturated CuN<sub>2</sub>S<sub>1</sub> site accelerated the initial oxygen reduction process, which in turn promoted catechol oxidation, thereby endowing ATT-Cu with a superior CO-like activity that surpassed that of a control nanozyme with a CuN<sub>1</sub>S<sub>3</sub> moiety and those of many CO-mimicking artificial enzymes/nanozymes with Cu–N<sub>x</sub>O<sub>y</sub> moieties as well as those of other Zr-based, Ce-based or Pt-based nanozymes.

## Results and discussion

Considering that the active site of natural CO involved Cu,<sup>18</sup> we chose Cu as the coordination center atom. To construct a nanozyme with a CuN<sub>x</sub>S<sub>y</sub> moiety, two ligands, *i.e.*, 3-thiol-1,2,4-triazole (TT) and 3-amino-5-thiol-1,2,4-triazole (ATT), were used to synthesize nanozymes (TT-Cu and ATT-Cu, Scheme 1) through a simple one-step coordination reaction between the ligands and CuSO<sub>4</sub> in water at room temperature. (See the Experimental section in ESI†) The only difference between TT and ATT was whether there existed an amino group, which was introduced to perturb the coordination microenvironment, thus modulating the coordination configuration of the Cu center.

A transmission electron microscope (TEM) was first used to observe the morphologies of TT-Cu and ATT-Cu. Interconnected nanoparticles with average sizes of 15.4 nm and 42.2 nm were observed for TT-Cu and ATT-Cu (Fig. 1A and B), respectively. The larger size of ATT-Cu could probably be attributed to the existence of –NH<sub>2</sub> in the ATT ligand, contributing to forming an extra H-bond network.<sup>19</sup> Such a morphology with the formation of interconnected nanoparticles was also confirmed by scanning electron microscope (SEM) (Fig. 1C and S1†). The survey scan spectra of X-ray photoelectron spectroscopy (XPS) detected the elemental signals of C, N, O, S and Cu (Fig. S2†), which were uniformly distributed in both nanozymes based on energy dispersive spectroscopy (EDS) mapping images (Fig. 1D and S3†). The results of inductively coupled plasma optical emission spectrometry (ICP-OES) indicated that the Cu contents in TT-Cu

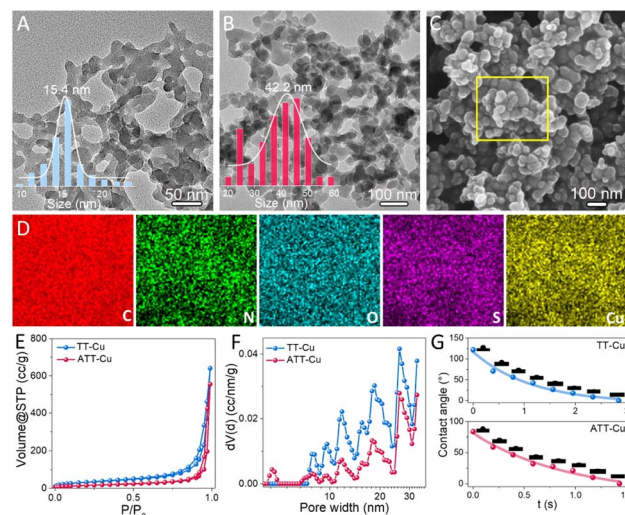
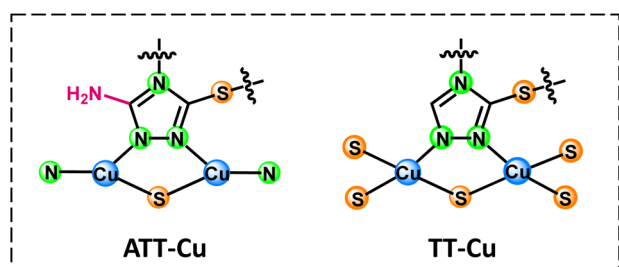


Fig. 1 TEM images of TT-Cu (A) and ATT-Cu (B); SEM image (C) and EDS mapping (D) of ATT-Cu; N<sub>2</sub> adsorption–desorption (E) and pore size distribution (F) curves of ATT-Cu and TT-Cu; (G) contact angles of ATT-Cu and TT-Cu.

and ATT-Cu were 43.9% and 31.9% (Fig. S4†), respectively. According to an N<sub>2</sub> adsorption/desorption experiment, we found that introducing the amino group caused a reduced surface area and pore volume in ATT-Cu compared with those of TT-Cu (Fig. 1E), although both showed similar mesopore-dominated porous structures (Fig. 1F). Meanwhile, both ATT-Cu and TT-Cu exhibited hydrophilic features (Fig. 1G), which would endow the active sites with an easy accessibility for hydrated O<sub>2</sub> during CO-mimicking catalysis.<sup>20</sup>

The collected N 1s spectra displayed that most N atoms in the TT ligand coordinated with Cu to form Cu–N bonds, in addition to the presence of a few uncoordinated N (Fig. 2A). Likewise, the formation of Cu–N bonds was also found for ATT-Cu (Fig. 2A). Differing from TT-Cu, another signal in the N 1s spectrum of ATT-Cu was also observed, which probably corresponded to exocyclic –NH<sub>2</sub>.<sup>21</sup> The calculated ratio of Cu–N and C–NH<sub>2</sub> was close to 3, implying that Cu possibly tended to coordinate with heterocyclic N atoms rather than exocyclic –NH<sub>2</sub>. This result was attributable to the weak Lewis basic feature of –NH<sub>2</sub> in the ATT ligand,<sup>22</sup> probably resulting in the poorer coordination ability of –NH<sub>2</sub>.<sup>23</sup> The O 1s spectra of ATT-Cu and TT-Cu detected H<sub>2</sub>O and SO<sub>4</sub><sup>2–</sup> originating from CuSO<sub>4</sub> (Fig. S5†). In the S 2p spectra, the important Cu–S signals were observed for both nanozymes apart from C–S and SO<sub>4</sub><sup>2–</sup> (Fig. 2B),<sup>24</sup> confirming the occurrence of coordination between Cu and the S atom of the ligand.

To further confirm the existence of Cu–N and Cu–S coordination, time-of-flight secondary ion mass spectrometry (ToF-SIMS) was conducted to disclose coordination information about the Cu center by identifying the mass fragments ejected from ATT-Cu and TT-Cu. In Fig. 2C, the characteristic fragment ions with mass-to-charge ratios (*m/z*) of 255.8 (Cu<sub>3</sub>C<sub>2</sub>N<sub>3</sub>H<sub>1</sub>) and 287.7 (Cu<sub>3</sub>C<sub>2</sub>N<sub>3</sub>S<sub>1</sub>H<sub>1</sub>) were detected for ATT-Cu, which may be assigned to Cu<sub>3</sub>-coordinated ATT fragments involving Cu–N and



Scheme 1 Coordination configurations of atomic Cu sites in ATT-Cu and TT-Cu. Note that only the structures of ligands and local motifs around Cu centers are presented for simplicity.



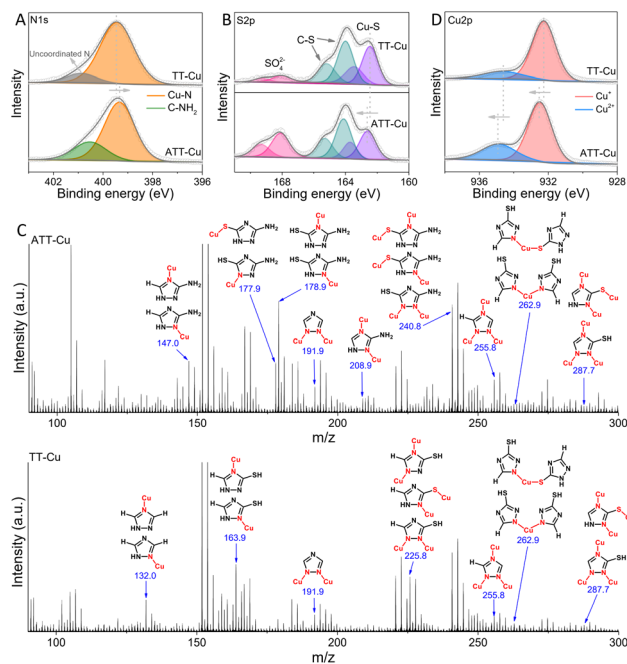


Fig. 2 N 1s (A) and S 2p (B) XPS spectra of ATT-Cu and TT-Cu; (C) ToF-SIMS analysis of ATT-Cu and TT-Cu and possible fragment assignments; (D) Cu 2p XPS spectra of ATT-Cu and TT-Cu.

Cu-S coordination, indicating that the S atom and three heterocyclic N atoms of ATT could bond with Cu. The possible existence of Cu-N and/or Cu-S coordination in the Cu<sub>2</sub>-coordinated ATT fragment ions, featuring *m/z* of 191.9 (Cu<sub>2</sub>C<sub>2</sub>N<sub>3</sub>), 208.9 (Cu<sub>2</sub>C<sub>2</sub>N<sub>4</sub>H<sub>3</sub>) and 240.8 (Cu<sub>2</sub>C<sub>2</sub>N<sub>4</sub>S<sub>1</sub>H<sub>3</sub>), as well as the Cu<sub>1</sub>-coordinated ATT fragments with *m/z* of 147.0 (Cu<sub>1</sub>C<sub>2</sub>N<sub>4</sub>H<sub>4</sub>), 177.9 (Cu<sub>1</sub>C<sub>2</sub>N<sub>4</sub>S<sub>1</sub>H<sub>3</sub>), 178.9 (Cu<sub>1</sub>C<sub>2</sub>N<sub>4</sub>S<sub>1</sub>H<sub>4</sub>) and 262.9 (Cu<sub>1</sub>C<sub>4</sub>-N<sub>6</sub>S<sub>2</sub>H<sub>4</sub>) supported coordination mainly occurring between the heterocyclic N and S atoms of ATT and Cu. Similar to ATT-Cu, the Cu<sub>1</sub>/Cu<sub>2</sub>/Cu<sub>3</sub>-coordinated TT fragments involving Cu-N and/or Cu-S coordination were also found for TT-Cu. These ToF-SIMS data, together with the XPS results, physically demonstrated that the three heterocyclic N atoms and S atoms of ATT/TT tended to coordinate with Cu to form CuN<sub>x</sub>S<sub>y</sub> configurations.

To explore how the coordinated N/S atoms in ATT and TT affected the electronic state of Cu, we collected the Cu 2p XPS spectra of ATT-Cu and TT-Cu (Fig. 2D). The Cu<sup>+</sup> and Cu<sup>2+</sup> species coexisted in both ATT-Cu and TT-Cu. Importantly, the binding energy of Cu in ATT-Cu was shifted positively compared with that in TT-Cu, verifying the accumulation of more positive charges at the Cu center of ATT-Cu. In Cu K-edge X-ray absorption near-edge structure (XANES) spectroscopy, the absorption edge energies of both ATT-Cu and TT-Cu were higher than that of Cu foil (Fig. 3A), indicating that Cu was in the oxidized state in both nanozymes.<sup>21</sup> Compared with TT-Cu, the absorption edge energy of ATT-Cu was shifted positively, and the intensity of the white line peak corresponding to the 1s → 4p<sub>xy</sub> transition also increased (Fig. 3A).<sup>25</sup> These results reconfirmed the accumulation of more positive charges at the

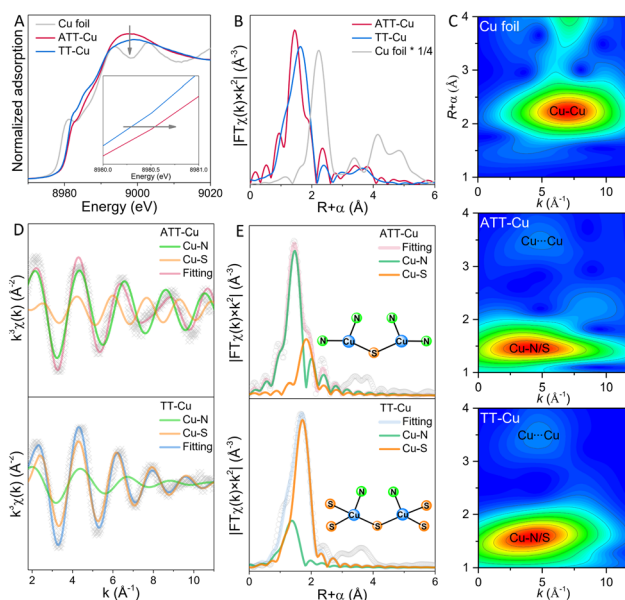


Fig. 3 X-ray absorption spectra of ATT-Cu, TT-Cu and Cu foil. (A) Cu K-edge XANES spectra; (B) Fourier-transform EXAFS curves in *R* space; (C) wavelet-transform EXAFS spectra; Fourier-transform EXAFS fitting curves in *k*-space (D) and *R*-space (E).

Cu center of ATT-Cu, agreeing well with the Cu 2p XPS result. Upon rechecking the N 1s and S 2p XPS spectra, we found that the Cu-N bond in ATT-Cu was shifted to a higher binding energy than that in TT-Cu, while the binding energy of the Cu-S bond in ATT-Cu was lower than that in TT-Cu (Fig. 2A and B). These results together with the Cu 2p and Cu K-edge XANES spectra illustrated that the more electrons of the Cu-N bond in ATT-Cu flowed toward the S atom compared with TT-Cu, causing more positive charges to accumulate at the Cu center of ATT-Cu.

To gain an insight into the origin of charge accumulation at the Cu center, extended X-ray absorption fine structure (EXAFS) spectroscopy was conducted to investigate the atomic-scale coordination configuration of Cu. As shown in Fig. 3B, the characteristic peaks of ATT-Cu and TT-Cu in Fourier-transform EXAFS spectra in *R* space were located at about 1.44 and 1.66 Å, respectively, and no Cu-Cu scattering peak at ~2.24 Å was observed for them, suggesting that the Cu atom of ATT-Cu and TT-Cu existed in the form of atomic dispersion. In wavelet transform (WT)-EXAFS spectra (Fig. 3C), the intensity maximum for ATT-Cu and TT-Cu were situated at about 3.90 Å<sup>-1</sup> and 4.05 Å<sup>-1</sup>, respectively, which were clearly different from that for Cu foil (7.05 Å<sup>-1</sup>), again supporting the atomic dispersion of Cu in both nanozymes. Additionally, we observed another prominent scattering path at ~3.48 Å in WT-EXAFS (Fig. 3C), which could possibly be assigned to the nonbonded Cu...Cu scattering originating from the adjacent geminal copper centers, similar to the reported triazole-Cu complex.<sup>19,21</sup>

The Fourier-transform EXAFS signal in *k*-space revealed that both ATT-Cu and TT-Cu presented two different oscillation periods, which corresponded to the Cu-N and Cu-S paths (Fig. 3D). This favored the formation of Cu-N and Cu-S



coordination, coinciding with the results of the N 1s/S 2p spectra and ToF-SIMS data. We thus performed Fourier-transform EXAFS fitting analysis in *R* space to determine the first-shell N/S atom numbers around the Cu center (Fig. 3E and Table S1†). For ATT-Cu, the average number of S atoms coordinating with Cu was 0.5, suggesting that each S atom was shared by two Cu atoms. Meanwhile, each Cu atom in ATT-Cu was also connected with two N atoms. Therefore, the Cu center of the ATT-Cu nanozyme formed the coordination-unsaturated  $\text{CuN}_2\text{S}_1$  configuration. In contrast to ATT-Cu, each Cu center in TT-Cu bonded with one N atom, and the average number of S atoms coordinating with Cu attained 2.5, suggesting that the adjacent two Cu atoms shared five S atoms, thus forming the  $\text{CuN}_1\text{S}_3$  coordination configuration in the TT-Cu nanozyme. These XANES and EXAFS data, together with the XPS and ToF-SIMS results as well as the different coordination structures of the nanozymes illustrated that introducing an amino group into the ATT ligand could modulate the coordination-unsaturated configuration of atomically dispersed Cu centers by steering the first-shell N/S atom numbers, thus promoting the more notable accumulation of positive charge at the Cu center of ATT-Cu.

The CO-like catalytic activities of ATT-Cu and TT-Cu were evaluated using 3,5-di-*tert*-butylcatechol (3,5-DBTC) as a model molecule.<sup>2</sup> In the absence of nanozyme, 3,5-DBTC in an air-saturated solution showed a characteristic absorption peak at 280 nm (Fig. 4A). Once the ATT-Cu nanozyme was introduced into the reaction solution, a new absorption peak located at 416 nm appeared, which was assigned to the oxidation product (*i.e.*, 3,5-di-*tert*-butyl-*o*-benzoquinone, 3,5-DTBQ) (Fig. 4A). When the reaction solution containing ATT-Cu was filtered using a filtration membrane with an average pore size of 100 nm, the reaction rate in this system obviously decreased (Fig. S6†). Meanwhile, increasing the  $\text{O}_2$  concentration accelerated the CO-mimicking catalysis of ATT-Cu, suggesting that ATT-Cu activated  $\text{O}_2$  to oxidize 3,5-DBTC (Fig. S7†). These results jointly verified the CO-mimicking activity of the ATT-Cu

nanozyme. Moreover, the CO-like activity of ATT-Cu increased with the increasing pH of the solution (Fig. S8†). For comparison with reported CO-like nanozymes,<sup>2,10</sup> a solution of pH = 8 was used. Additionally, we found that sodium metabisulfite ( $\text{Na}_2\text{S}_2\text{O}_5$ ) acting as an inhibitor could significantly inhibit the catalytic activity of ATT-Cu nanozyme (Fig. S9A†), analogous to reported CO and CO-like nanozymes.<sup>21,26</sup>

Interestingly, compared with ATT-Cu, TT-Cu displayed poor CO-mimicking activity (Fig. 4A), as demonstrated by its lower specific activity (Fig. 4B). Moreover, both the Cu content and the surface area of ATT-Cu were lower than those of TT-Cu, manifesting that the Cu content and surface area were not the crucial causes dominating the different CO-like activities between ATT-Cu and TT-Cu. To further compare the difference in intrinsic catalytic activities between ATT-Cu and TT-Cu, kinetic parameters such as substrate affinity ( $K_m$ ), catalytic rate constant ( $K_{\text{cat}}$ ) and catalytic efficiency ( $K_{\text{cat}}/K_m$ ) were assessed at room temperature under the condition of pH = 8 by varying the initial concentration of 3,5-DTBC. The catalytic reaction rates of both ATT-Cu and TT-Cu nanozymes followed Michaelis–Menten kinetics while performing CO-like catalysis (Fig. 4C), analogous to reported CO-mimicking nanozymes.<sup>2,10</sup> According to the Michaelis–Menten equation,  $K_m$ ,  $K_{\text{cat}}$  and  $K_{\text{cat}}/K_m$  were acquired through non-linear curve fitting. ATT-Cu exhibited better substrate affinity, as confirmed by its lower  $K_m$  value compared with TT-Cu (Fig. 4D). The  $K_{\text{cat}}$  and  $K_{\text{cat}}/K_m$  values of ATT-Cu were obviously superior to those of TT-Cu, demonstrating the better CO-mimicking activity of ATT-Cu (Fig. 4D). After five catalytic cycles, the CO-like activity of the ATT-Cu nanozyme did not notably decrease (Fig. 4E), indicating its good recyclability. Moreover, the corresponding XRD pattern of ATT-Cu did not show a notable difference compared with the original ATT-Cu (Fig. S9B†). Meanwhile, adding interfering ions such as  $\text{K}^+$ ,  $\text{Na}^+$  or  $\text{Cl}^-$  also did not result in a notable decrease in the catalytic activity of ATT-Cu (Fig. S9C†). Importantly, some of these kinetic parameters presented by this ATT-Cu nanozyme with a low-coordinated  $\text{CuN}_2\text{S}_1$  configuration surpassed those of many reported CO-mimicking artificial enzymes/nanozymes with  $\text{CuN}_x\text{O}_y$  moieties<sup>10,15</sup> as well as those of Ce-based,<sup>2,27</sup> Zr-based<sup>27</sup> or Pt-based<sup>2</sup> nanozymes (Fig. 4F and Table S2†). This demonstrated that using large-sized and weakly electronegative S as a coordinating atom could endow the Cu center with superior CO-like activity when the N/S coordination numbers were controlled to manipulate the coordination unsaturation of the Cu center to modulate its charge accumulation.

To explore why this low-coordinated  $\text{CuN}_2\text{S}_1$  configuration with accumulation of more positive charges at the Cu center accelerated the CO-mimicking catalysis of ATT-Cu, we first used electrochemical technology to understand this biomimetic oxidation process. According to the cyclic voltammetry (CV) curve acquired in the absence of  $\text{O}_2$ , it could be seen that the potential for oxidizing 3,5-DTBC over ATT-Cu was lower than that over TT-Cu (Fig. 5A), indicating that accumulation of more positive charges at the Cu center endowed ATT-Cu with easier reception of electrons during the oxidation of 3,5-DTBC. However, the ATT-Cu nanozyme showed a lower redox constant ( $k_s$ ) determined in the absence of  $\text{O}_2$  based on Laviron's method

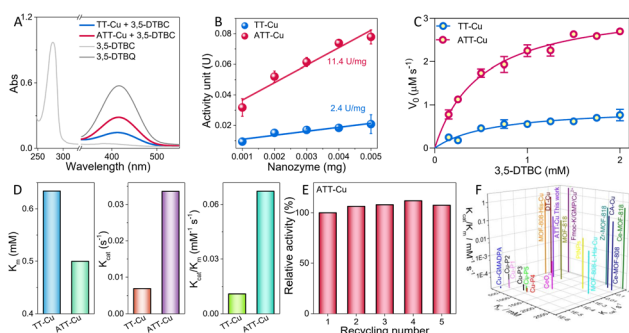
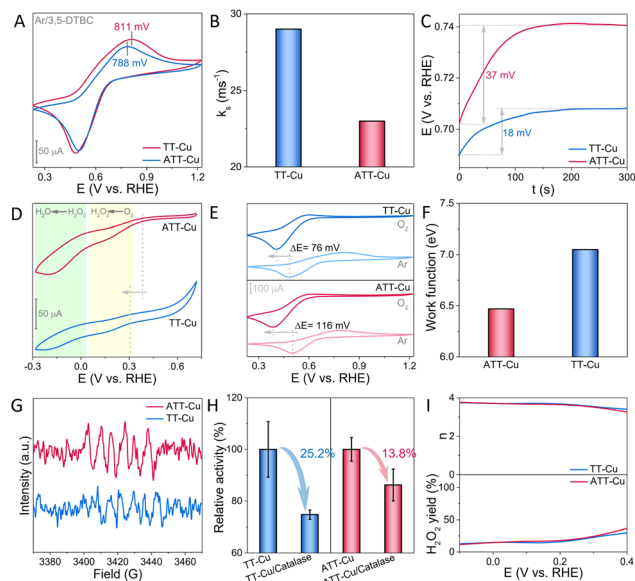


Fig. 4 Evaluation of CO-like activities of ATT-Cu and TT-Cu. (A) UV-vis spectra of 3,5-DTBC, 3,5-DTBQ and nanozyme-catalyzed oxidation of 3,5-DTBC in air-saturated PBS (pH = 8)/CH<sub>3</sub>CN solution; (B) specific activities; (C) Michaelis–Menten curves; (D) kinetic parameters ( $K_m$ ,  $K_{\text{cat}}$  and  $K_{\text{cat}}/K_m$ ); (E) recyclability; (F) comparison of the kinetic parameters ( $K_m$ ,  $K_{\text{cat}}$  and  $K_{\text{cat}}/K_m$ ) of ATT-Cu with reported CO-like artificial enzymes.





**Fig. 5** (A) CV curves of ATT-Cu and TT-Cu in the presence of Ar and 3,5-DTBC; (B)  $k_s$  values of ATT-Cu and TT-Cu during oxidation of 3,5-DTBC based on Laviron analysis; (C) changes in OCP over time; (D) CV curves of ATT-Cu and TT-Cu in the presence of  $O_2$ ; (E) CV curves of ATT-Cu and TT-Cu in the presence of 3,5-DTBC as well as  $O_2$  or Ar; (F) work functions of ATT-Cu and TT-Cu; (G) ESR spectra of DMPO-trapped  $O_2^{\bullet-}$ ; (H) specific trapping of  $H_2O_2$  during ATT-Cu- and TT-Cu-catalyzed oxidation of 3,5-DTBC using catalase; (I) electron transfer numbers ( $n$ ) and  $H_2O_2$  yields of ATT-Cu and TT-Cu during ORR.

(Fig. 5B and S10†),<sup>28</sup> suggesting the slower oxidation rate of 3,5-DTBC over ATT-Cu compared with that over TT-Cu. In fact, the catalytic kinetics experiment disclosed that ATT-Cu exhibited a faster rate for oxidizing 3,5-DTBC compared with TA-Cu while performing CO-like catalysis (Fig. 4C and D). This implied that the process of the oxygen reduction reaction (ORR) should be the key initial step for controlling CO-like catalysis, rather than the oxidation step of 3,5-DTBC.

If the above deduction was reasonable, the preferentially triggered ORR process would make the Cu center of the nanozyme become more electron-deficient, thus elevating the electrochemical potential of the Cu site to accelerate 3,5-DTBC oxidation. Meanwhile, this rising electrochemical potential would also make the nanozyme a weaker reductant, attenuating the ORR rate. Accordingly, the “mixed potential” of reductive and oxidative half-reactions (*i.e.*, the open-circuit potential (OCP))<sup>29</sup> would experience a continuous change until the rates of ORR and oxidation of 3,5-DTBC were balanced to attain a steady state, which coincided with Fig. 5C, demonstrating that the ORR process was the key initial step during CO-mimicking catalysis. Furthermore, compared with TT-Cu, ATT-Cu showed a more notable change in OCP when reaching a steady state (Fig. 5C), signifying that the initial ORR step driven by ATT-Cu was faster. Fig. 5D verified this, showing that the onset potential and current of ORR over ATT-Cu exceeded those over TT-Cu. Combining these results and the above structural information indicated that accumulating more positive charges at the low-

coordinated  $CuN_2S_1$  site contributed to boosting the CO-mimicking activity of ATT-Cu by accelerating the key initial ORR step.

To clarify the origin of the faster ORR step exhibited by ATT-Cu, we compared the CV curves of the two nanozymes, which were collected in the presence of 3,5-DTBC as well as Ar or  $O_2$ , respectively. We found that introducing  $O_2$  into the reaction system resulted in the disappearance of the oxidation peak of 3,5-DTBC, and the reduction peak of 3,5-DTBQ (*i.e.* the oxidation product of 3,5-DTBC) was negatively shifted (Fig. 5E), which illustrated that the electrochemical oxidation of 3,5-DTBC and the reduction of 3,5-DTBQ became more difficult in the presence of  $O_2$ , suggesting that  $O_2$  may be more easily preferentially adsorbed by both nanozymes to occupy their Cu sites. It is worth noting that after replacing Ar with  $O_2$ , the 3,5-DTBQ reduction peak presented by ATT-Cu was negatively shifted by 116 mV, which obviously exceeded that shown by TT-Cu (76 mV) (Fig. 5E), reflecting the stronger adsorption of  $O_2$  by ATT-Cu during CO-like catalysis. After  $O_2$  was adsorbed, the lower work function of ATT-Cu enabled an easier electron transfer to  $O_2$  (Fig. 5F). These factors ensured the formation of more  $O_2^{\bullet-}$  species, which were confirmed in the presence of air and 5,5-dimethyl-1-pyrroline *N*-oxide (DMPO) without adding 3,5-DTBC through electron spin resonance (ESR) spectra (Fig. 5G).

As the ORR process progressed, this formed  $O_2^{\bullet-}$  would be further transformed into the product  $H_2O$  *via* the formation of  $H_2O_2$  intermediate by further accepting electrons stemming from oxidation of 3,5-DTBC during CO-mimicking catalysis, as shown by the result of a catalase trapping experiment (Fig. 5H) and the evaluated electron transfer number approaching 4 (Fig. 5I). Such a 4e reduction of  $O_2$  to form  $H_2O$  *via* the  $H_2O_2$  intermediate was also confirmed by the CV curve. It displayed two obvious stages corresponding to  $O_2 \rightarrow H_2O_2 \rightarrow H_2O$  during the nanozyme-catalyzed ORR process (Fig. 5D). Moreover, according to Fig. 5H, we found that the drop in the relative CO-like activity of ATT-Cu was smaller than that of TT-Cu after adding catalase into the reaction system. Given that catalase specifically competed with the nanozyme for  $H_2O_2$ , the smaller decrease in relative CO-like activity demonstrated the stronger adsorption capability of ATT-Cu for  $H_2O_2$ . As a result, the stronger capabilities for adsorbing  $O_2$  and  $H_2O_2$  intermediate as well as the faster electron transfer jointly enabled the ATT-Cu nanozyme to exhibit better ORR activity than TT-Cu, as confirmed by its more positive onset potential and larger current for ORR (Fig. 5D). Such an enhanced ORR process contributed to boosting the CO-mimicking activity of ATT-Cu.

To further understand why the ATT-Cu nanozyme with more accumulated positive charges enabled by the low-coordinated  $CuN_2S_1$  configuration enhanced adsorption of  $O_2$  and  $H_2O_2$  intermediates, an ultraviolet photoelectron spectroscopy (UPS) test was conducted to evaluate its d-band center. In general, upshifting the d-band center of a catalyst is beneficial for enhancing the adsorption strength of a catalyst for reactive species. As expected, the d-band center of ATT-Cu was upshifted toward the Fermi level compared to that of TT-Cu (Fig. 6A), contributing to enhanced  $O_2/H_2O_2$  adsorption. Furthermore, this upshifted d-band center prompted the ATT-Cu nanozyme



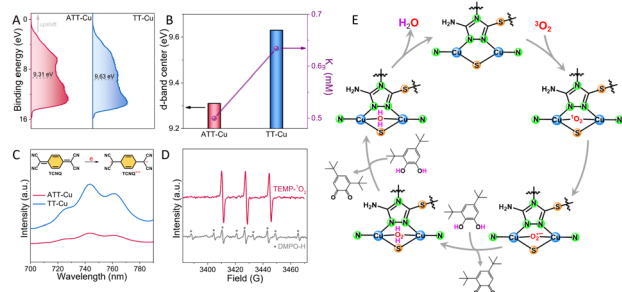


**Fig. 6** (A) UPS spectra of ATT-Cu and TT-Cu; (B) positive relationship between d-band center and  $K_m$  of ATT-Cu and TT-Cu; (C) UV-vis spectra of TCNQ solutions in the presence of ATT-Cu and TT-Cu; (D) trapping other reactive oxygen species ( $\cdot\text{OH}$  and  $^1\text{O}_2$ ) during the biomimetic oxidation of 3,5-DTBC over ATT-Cu; 2,2,6,6-tetramethylpiperidine (TEMP) and 5,5-dimethyl-1-pyrroline *N*-oxide (DMPO) were used to trap  $^1\text{O}_2$  and  $\cdot\text{OH}$ , respectively; note: the  $\cdot\text{OH}$  signal was inconspicuous, and the DMPO-H adduct and TEMPO were found; (E) proposed catalytic mechanism of ATT-Cu.

to present better affinity for 3,5-DTBC, as shown by its lower  $K_m$  value (Fig. 6B).

Once 3,5-DTBC was adsorbed, the nanozyme would catalyze the oxidation of 3,5-DTBC by accepting its electron. To compare their capabilities for accepting electrons, 7,7,8,8-tetracyanoquinodimethane (TCNQ) was employed as a probe molecule to mix with the nanozyme in acetonitrile solution. After stirring at 80 °C for 20 min, the centrifuged solution was monitored using UV-vis spectra. A peak at 743 nm was observed (Fig. 6C), suggesting that TCNQ accepted one electron from the nanozyme to form the radical anion product  $\text{TCNQ}^{\cdot-}$ .<sup>30,31</sup> However, this  $\text{TCNQ}^{\cdot-}$  peak in the ATT-Cu system was much weaker than that in the TT-Cu system (Fig. 6C), indicating that the ATT-Cu nanozyme found it harder to donate an electron to TCNQ compared with TT-Cu. In other words, the capability of ATT-Cu to accept an electron was stronger than that of TT-Cu, which agreed well with the lower potential of ATT-Cu for the oxidation of 3,5-DTBC (Fig. 5A). Consequently, the better capability to accept and transfer electrons as well as the stronger adsorption for  $\text{O}_2$ ,  $\text{H}_2\text{O}_2$  and 3,5-DTBC physically enabled ATT-Cu with a low-coordinated  $\text{CuN}_2\text{S}_1$  moiety to accelerate CO-like catalysis.

To disclose the possible biomimetic catalytic mechanism of ATT-Cu, we further used electron paramagnetic resonance (EPR) to trap other reactive oxygen species (*i.e.*  $\cdot\text{OH}$  and  $^1\text{O}_2$ ) apart from the detected  $\text{O}_2^{\cdot-}$  and  $\text{H}_2\text{O}_2$ . 2,2,6,6-Tetramethylpiperidine (TEMP) and 5,5-dimethyl-1-pyrroline *N*-oxide (DMPO) were used as trapping reagents for  $^1\text{O}_2$  and  $\cdot\text{OH}$ , respectively. As shown in Fig. 6D, an obvious TEMPO signal was observed while the DMPO-OH signal was inconspicuous, suggesting that  $^1\text{O}_2$  was involved in the oxygen activation process and  $\cdot\text{OH}$  was possibly not formed. On the basis of these detected reactive oxygen species, a possible catalytic mechanism was proposed (Fig. 6E). During catalysis, ATT-Cu preferentially adsorbed and activated  $\text{O}_2$  to form  $^1\text{O}_2$ , which would be transformed into  $\text{O}_2^{\cdot-}$ . The formed  $\text{O}_2^{\cdot-}$  would be transformed into  $\text{H}_2\text{O}_2$  by accepting electrons and hydrogen atoms from 3,5-DTBC, thus generating the oxidation product (*i.e.*, 3,5-DTBQ). The produced  $\text{H}_2\text{O}_2$  was

further transformed into  $\text{H}_2\text{O}$  by obtaining electrons and hydrogen atoms from 3,5-DTBC to produce  $\text{H}_2\text{O}$  and 3,5-DTBQ. Subsequently, the Cu site of ATT-Cu experienced a regeneration process by desorbing the resulting  $\text{H}_2\text{O}$ .

## Conclusions

In summary, we constructed CO-like nanozymes with  $\text{CuN}_2\text{S}_1$  and  $\text{CuN}_1\text{S}_3$  moieties by steering the N/S coordination number around Cu centers. We found that the d-band center of ATT-Cu with the low-coordinated  $\text{CuN}_2\text{S}_1$  configuration was upshifted toward the Fermi level compared with that of TT-Cu with the  $\text{CuN}_1\text{S}_3$  moiety, leading to stronger adsorption of  $\text{O}_2$  and  $\text{H}_2\text{O}_2$  intermediates as well as better affinity for catechol. Meanwhile, this unsaturated  $\text{CuN}_2\text{S}_1$  configuration provided ATT-Cu with better capabilities for donating electrons to  $\text{O}_2$  and accepting electrons from catechol. These advantages accelerated the initial ORR process, which in turn promoted the oxidation of catechol, thus endowing ATT-Cu with enhanced CO-like activity.

## Data availability

The data that supports the findings of this study is available from the corresponding author upon reasonable request.

## Author contributions

F. H. conceived and designed the experiments. M. Y. and Z. H. performed the synthesis and/or activity evaluation of nanozyme. N. X. and C. H. provided assistance with the funding. F. H. wrote and revised the manuscript. F. H. and X. H. supervised the project.

## Conflicts of interest

The authors declare no competing financial interests.

## Acknowledgements

This work was financially supported by Doctoral Fund Project of University of Jinan (XBS2409), the Foundation (No. GZKF202335) of State Key Laboratory of Biobased Material and Green Papermaking (Qilu University of Technology, Shandong Academy of Sciences), National Natural Science Foundation of China (No. 52276195 and No. 22408190), Program for Supporting Innovative Research from Jinan (202228072) and Program of Agricultural Development from Shandong (SD2019NJ015). The authors extend their gratitude to Mr Yanda Du from Shiyanjia Lab (<https://www.shiyanjia.com>) for providing invaluable assistance with the XPS analysis.

## References

- 1 S. Ji, B. Jiang, H. Hao, Y. Chen, J. Dong, Y. Mao, Z. Zhang, R. Gao, W. Chen and R. Zhang, *Nat. Catal.*, 2021, **4**, 407–417.



- 2 M. Li, J. Chen, W. Wu, Y. Fang and S. Dong, *J. Am. Chem. Soc.*, 2020, **142**, 15569–15574.
- 3 G. Li, H. Liu, T. Hu, F. Pu, J. Ren and X. Qu, *J. Am. Chem. Soc.*, 2023, **145**, 16835–16842.
- 4 D. Chen, Z. Xia, Z. Guo, W. Gou, J. Zhao, X. Zhou, X. Tan, W. Li, S. Zhao, Z. Tian and Y. Qu, *Nat. Commun.*, 2023, **14**, 7127.
- 5 Y. Xu, Y. Ma, X. Chen, K. Wu, K. Wang, Y. Shen, S. Liu, X. Gao and Y. Zhang, *Angew. Chem., Int. Ed.*, 2024, e202408935.
- 6 K. Wang, Q. Hong, C. Zhu, Y. Xu, W. Li, Y. Wang, W. Chen, X. Gu, X. Chen, Y. Fang, Y. Shen, S. Liu and Y. Zhang, *Nat. Commun.*, 2024, **15**, 5705.
- 7 Y. Hu, X. J. Gao, Y. Zhu, F. Muhammad, S. Tan, W. Cao, S. Lin, Z. Jin, X. Gao and H. Wei, *Chem. Mater.*, 2018, **30**, 6431–6439.
- 8 F. Cao, H. Feng, J. Yao, X. Hou, T. Jin and J. Hui, *Nano Res.*, 2024, **17**, 6376–6385.
- 9 Y. Chen, B. Jiang, H. Hao, H. Li, C. Qiu, X. Liang, Q. Qu, Z. Zhang, R. Gao, D. Duan, S. Ji, D. Wang and M. Liang, *Angew. Chem., Int. Ed.*, 2023, **62**, e202301879.
- 10 M. Sha, L. Rao, W. Xu, Y. Qin, R. Su, Y. Wu, Q. Fang, H. Wang, X. Cui and L. Zheng, *Nano Lett.*, 2023, **23**, 701–709.
- 11 S. Xu, H. Wu, S. Liu, P. Du, H. Wang, H. Yang, W. Xu, S. Chen, L. Song and J. Li, *Nat. Commun.*, 2023, **14**, 4040.
- 12 Y. Lin, F. Wang, J. Yu, X. Zhang and G. P. Lu, *J. Hazard. Mater.*, 2022, **425**, 127763.
- 13 P. Makam, S. S. Yamijala, V. S. Bhadram, L. J. Shimon, B. M. Wong and E. Gazit, *Nat. Commun.*, 2022, **13**, 1505.
- 14 W. Zou, Y. Liu, R. Li and R. Guo, *ACS Sustain. Chem. Eng.*, 2022, **10**, 10057–10067.
- 15 S. Thanneeru, N. Milazzo, A. Lopes, Z. Wei, A. M. Angeles-Boza and J. He, *J. Am. Chem. Soc.*, 2019, **141**, 4252–4256.
- 16 H. Shang, X. Zhou, J. Dong, A. Li, X. Zhao, Q. Liu, Y. Lin, J. Pei, Z. Li, Z. Jiang, D. Zhou, L. Zheng, Y. Wang, J. Zhou, Z. Yang, R. Cao, R. Sarangi, T. Sun, X. Yang, X. Zheng, W. Yan, Z. Zhuang, J. Li, W. Chen, D. Wang, J. Zhang and Y. Li, *Nat. Commun.*, 2020, **11**, 3049.
- 17 K. Li and D. Xue, *J. Phys. Chem. A*, 2006, **110**, 11332–11337.
- 18 T. Klabunde, C. Eicken, J. C. Sacchettini and B. Krebs, *Nat. Struct. Biol.*, 1998, **5**, 1084–1090.
- 19 E. Aznar, S. Ferrer, J. Borrás, F. Lloret, M. Liu-González, H. Rodríguez-Prieto and S. García-Granda, *Eur. J. Inorg. Chem.*, 2006, 5115–5125.
- 20 G.-P. Hao, N. R. Sahraie, Q. Zhang, S. Krause, M. Oschatz, A. Bachmatiuk, P. Strasser and S. Kaskel, *Chem. Commun.*, 2015, **51**, 17285–17288.
- 21 M. Yuan, K. Han, H. Yang, L. Mi, C. Huang, X. Hu and F. He, *Small*, 2024, e2401756.
- 22 H. S. Park, R. Sun, E. J. Lee, J. Kim and N. H. Hur, *ACS Omega*, 2022, **7**, 40860–40868.
- 23 Z. Shi, Y. Tao, J. Wu, C. Zhang, H. He, L. Long, Y. Lee, T. Li and Y.-B. Zhang, *J. Am. Chem. Soc.*, 2020, **142**, 2750–2754.
- 24 Q. Wen, Y. Lin, Y. Yang, R. Gao, N. Ouyang, D. Ding, Y. Liu and T. Zhai, *ACS Nano*, 2022, **16**, 9572–9582.
- 25 S. Li, P. Ma, C. Gao, L. Liu, X. Wang, M. Shakouri, R. Chernikov, K. Wang, D. Liu, R. Ma and J. Wang, *Energy Environ. Sci.*, 2022, **15**, 3004–3014.
- 26 M. Ü. Ünal, *Food Chem.*, 2007, **100**, 909–913.
- 27 S. Liu, Y. He, W. Zhang, T. Fu, L. Wang, Y. Zhang, Y. Xu, H. Sun and H. Zhao, *Small*, 2024, **20**, e2306522.
- 28 P. Ei Phyu Win, J. Yang, S. Ning, X. Huang, G. Fu, Q. Sun, X. H. Xia and J. Wang, *Proc. Natl. Acad. Sci. U. S. A.*, 2024, **121**, e2316553121.
- 29 W. C. Howland, J. B. Gerken, S. S. Stahl and Y. Surendranath, *J. Am. Chem. Soc.*, 2022, **144**, 11253–11262.
- 30 G. A. Saleh, *Talanta*, 1998, **46**, 111–121.
- 31 J. Song, Z. Ji, Q. Nie and W. Hu, *Nanoscale*, 2014, **6**, 2573–2576.

